PAPER

Isothermal titration calorimetry as a powerful tool to quantify and better understand agglomeration mechanisms during interaction processes between TiO₂ nanoparticles and humic acids†

Frédéric Loosli,[a] Letícia Vitorazi,[b] Jean-François Berret[b] and Serge Stoll*[a]

The association processes between engineered TiO₂ nanoparticles and Suwannee River humic acids are investigated by isothermal titration calorimetry and by measuring the exchanged heat during the binding process, allowing the determination of thermodynamic (change in enthalpy, Gibbs free energy and entropy) and reaction (binding affinity constant, reaction stoichiometry) parameters. Our results indicate that strong TiO₂–Suwannee River humic acid interactions are entropically and enthalpically favorable with exothermic binding reactions and that the mixing order is also an important parameter. High humic acid concentrations induce homoagglomeration ("self"-assembly) and are shown to favor an enthalpically driven association process. Light scattering techniques are also considered to investigate the influence of TiO₂ surface charge modifications and agglomeration mechanisms. Patch and bridging mechanisms are found to result in the formation of large agglomerates once charge inversion of TiO₂–humic acid complexes is achieved. Moreover, van der Waals interactions are also found to play a significant role during interaction processes due to the amphiphilic character of humic acids.

Nano impact

The stability of engineered nanoparticles in aquatic systems is strongly influenced by their interactions with aquagenic compounds such as natural organic matter. In order to have a better understanding of these interaction processes and the resulting agglomeration or stabilization mechanisms, isothermal titration calorimetry is proposed here as a promising and novel technique in the field of environmental science. This approach allows the thermodynamic quantification and determination of the agglomeration mechanism during association processes between TiO₂ nanoparticles and humic acids. Such an evolution in the comprehension of the interaction phenomena is an important step to improve our knowledge of the behavior of nanoparticles and the risk assessment associated to nanoparticles in aquatic systems.

1. Introduction

A better understanding of the fate and behavior of engineered nanoparticles (ENPs) in the presence of aquagenic compounds is of great importance for the risk assessment associated to ENPs entering environmental aquatic systems.[1–5] Indeed, nanomaterials are produced in large and growing amounts[6] due to their very unique electronic and surface chemistry properties.[7] ENPs are then expected to enter aquatic natural systems not only through surface runoff and accidental discharge but also due to the lack of efficiency in removing them in wastewater treatment plants.[8–10] Once in aquatic systems, ENP stability is strongly influenced by the physicochemical properties of water, *i.e.* pH, ionic strength,[11–13] ENP intrinsic properties, *i.e.* size, shape, surface charge and chemistry,[14,15] and the presence of aquagenic compounds such as natural colloids and living microorganisms.[16,17] Complex formation between ENPs and natural compounds strongly modifies the ENP stability, fate, transport, bioavailability and effect towards living organisms.[18,19]

An important class of organic colloids is represented by natural organic matter (NOM). The larger fraction of NOM is composed of humic substances with up to 30–50% of total surface water organic matter.[20] Humic substances are derived from plant and animal residues through humification

[a] *Group of Environmental Physical Chemistry, University of Geneva, F.-A. Forel Institute Section des Sciences de la Terre et de l'Environnement, 10 route de Suisse, 1290 Versoix, Switzerland. E-mail: serge.stoll@unige.ch; Fax: +41 22 379 0302; Tel: +41 22 379 0333*
[b] *Laboratoire Matière et Systèmes Complexes, UMR 7057 Université Paris-Diderot/ CNRS, Bâtiment Condorcet, 10 rue Alice Domon et Léonie Duquet, F-75205 Paris cedex 13, France*
† Electronic supplementary information (ESI) available. See DOI: 10.1039/c5en00139k

This journal is © The Royal Society of Chemistry 2015

Environ. Sci.: Nano, 2015, **2**, 541–550 | 541

processes.[21] The interaction processes between ENPs and the soluble fraction of humic substances (fulvic and humic acids) have been investigated in many studies.[22–24] Their presence was shown to deeply modify the ENP surface charge, resulting in stability through electrostatic interactions and steric effects once adsorbed on ENPs.[25–27] The presence of NOM was found not only to promote ENP agglomeration or stabilization but also to induce the partial fragmentation of already formed ENP agglomerates.[28–30] Agglomeration *versus* fragmentation was found to be dependent on the nature of NOM, ENP surface properties and the concentration ratio between them.

Most of these studies investigated the ENP stability for different experimental conditions by determining the ENP surface charge modification and the resulting state of agglomeration (size and fractal dimension) to understand the influence of pH, NOM properties, electrolyte concentration and valency. In the present study we focus on a different but important complementary aspect related to the quantification of the energies associated to the interaction processes and agglomeration mechanisms. Isothermal titration calorimetry (ITC) is used here to quantify the complexation between TiO_2 ENPs and humic acids. ITC is an instrumental technique which permits the determination, in a single experiment, of all interaction thermodynamic parameters (ΔH, ΔS and ΔG) and to provide information on the reaction stoichiometry and binding affinity. ITC has been applied to study binding reactions for the self-assembly of supramolecular polymers and protein–substrate interactions.[31–34] In this study we use a novel approach, *via* ITC measurements, to get a quantitative insight into the interaction energies between TiO_2 ENPs and humic acids. TiO_2 ENPs are one of the most produced nanomaterials,[6,35,36] being used in many industrial domains such as in the food, cosmetic and painting industries.[37–39] TiO_2 ENPs are likely to be already present in the natural aquatic systems in the ng L^{-1} to μg L^{-1} range.[9,40] The influence of NOM and water properties on their stability was thoroughly investigated.[41,42]

In the present study all thermodynamic reaction parameters associated to the complexation processes are considered together, in addition to ENP surface charge modification and size evolution, to propose a detailed quantification of the energy involved during interaction processes. Comparison is also made with dynamic light scattering and electrophoretic mobility measurements to obtain a better description of the agglomeration mechanisms (patch and bridging) between TiO_2 ENPs and humic acids.

2. Materials and methods

2.1. Materials

A 5 g L^{-1} TiO_2 dispersion was prepared by dilution of a 15 wt% TiO_2 suspension (obtained from Nanostructured & Amorphous Materials, Inc., Houston, TX, USA), after homogenization, with Milli-Q water (Millipore, Zoug, ZG, Switzerland, with R >18 MΩ cm, T.O.C. <2 ppb). NaOH and HCl (1 M, Titrisol®, Merck, Zoug, ZG, Switzerland) were used after

dilution to adjust the ENP dispersions at pH 3.8 and 10.4. The TiO_2 dispersion was then dialyzed against water (pH 3.8 and 10.4) with 12–14 kDa cutoff dialysis membranes (Spectrum Laboratories, Inc., Rancho Dominguez, CA, USA). Dialysis was realized to minimize the change in enthalpy due to the dilution processes during titration. The rather low molecular weight of SRHAs[43] does not allow their dialysis. The dialysis solvent was first used to prepare humic acid (Suwannee River humic acids (SRHAs), Standard II, International Humic Substances Society, Denver, CO, USA) solutions with concentrations equal to 1.25 mM in terms of charge concentration (600 mg L^{-1} for pH 3.8 and 201 mg L^{-1} for pH 10.4) which were stirred overnight. The water from dialysis was also used to dilute the TiO_2 and SRHA suspensions to experimental concentrations (from 0.1 to 3.5 g L^{-1} for TiO_2 and from 0.0375 to 0.75 mM for SRHA).

2.2. Isothermal titration calorimetry measurement

A VP-ITC calorimeter (MicroCal Inc., Northampton, MA, USA) with a sample cell volume equal to 1.4643 mL was used to determine the heat exchange between TiO_2 ENPs and SRHAs. After a preliminary injection of 2 μL of the first compound (ligand (L)), 28 successive injections of 10 μL into the sample cell containing the other compound of interest (macromolecule (M)) were realized with injection duration equal to 20 s and a delay of 300 s between two successive additions The stirring speed was set to 307 rpm and the working temperature to 298.15 K for all experiments. The plot of the heat of exchange (dQ/dn_L) as a function of the molar charge ratio (Z = [L]/[M], where [L] and [M] are the ligand and macromolecule molar charge concentration, respectively) is fitted with a multiple non-interacting sites (MNIS) model (eqn (1)) where the sites do not exhibit cooperative binding behavior.[44] In order to determine the fitting parameters, the following equation is used.

$$\frac{dQ}{dn_L}(Z) = \frac{1}{2}\Delta H_b\left[1 + \left(1 - \frac{[L]}{n[M]} - \frac{1}{nK_b[M]}\right)\left(\left(1 + \frac{[L]}{n[M]} + \frac{1}{nK_b[M]}\right)^2 - \frac{4[L]}{n[M]}\right)^{-\frac{1}{2}}\right]$$

(1)

In this equation, the fitting parameters are ΔH_b [kJ mol^{-1}], K_b [M^{-1}] and n, and they represent the binding enthalpy (energy involved during association processes), affinity binding constant (affinity between the two compounds) and reaction stoichiometry, respectively. These parameters are adjusted to fit the experimental curves with the mathematical MNIS model given by eqn (1). Then, the Gibbs free energy, ΔG [kJ mol^{-1}], and the change in entropy, ΔS [kJ K^{-1} mol^{-1}], are calculated from the fitting parameters with $\Delta G = -RT\ln K_b$

542 | *Environ. Sci.: Nano*, 2015, **2**, 541–550

This journal is © The Royal Society of Chemistry 2015

and $\Delta S = (\Delta H - \Delta G)/T$. The ligand and macromolecule charge numbers for the ith-injection are equal to:

$$L_i = L_{i-1} + V_i[L]_m N_A \text{ and } M = [M]_m V_{cell} N_A \quad (2)$$

with

$$[TiO_2]_m = [TiO_2]_M \, S_A \sigma_{TiO_2} \times 10^{18} \times \frac{1}{N_A} \quad (3)$$

and

$$[SRHA]_m = [SRHA]_M \, Q_{tot} \times 10^{-3} \times \frac{C\%}{100} \quad (4)$$

where

$$Q_{tot} = \left(\frac{Q_1}{1 + \left(K_1 \left[H^+ \right]^{\frac{1}{n_1}} \right)} \right) + \left(\frac{Q_2}{1 + \left(K_2 \left[H^+ \right]^{\frac{1}{n_2}} \right)} \right) \quad (5)$$

In eqn (2), V_i and V_{cell} represent the volume of ligand injected and the cell volume, respectively. $[L]_m$ or $[M]_m$ corresponds to the moles of charge of ligand or macromolecule per unit volume, respectively, and N_A is Avogadro's constant. The concentration in terms of moles of charge per unit volume for TiO₂ and SRHA are expressed in eqn (3) and (4), respectively. In eqn (3), $[TiO_2]_M$ represents the TiO₂ mass concentration, S_A the ENP specific surface area $[m^2 \, g^{-1}]$ and σ_{TiO_2} the TiO₂ hydroxyl site density [sites per nm²]. In eqn (4), $[SRHA]_M$ represents the SRHA mass concentration, Q_{tot} the SRHA overall charge density [meq g C⁻¹] and C% the SRHA percent of carbon, which is equal to 52.63%.[45] For the modified Henderson–Hasselbalch equation (eqn (5)), the values of maximum charge densities Q_1 and Q_2 of SRHA carboxylic and phenolic binding sites, the two dissociation constants K_1 and K_2 and empirical parameters n_1 and n_2 were taken from the study by Ritchie *et al.* dealing with the proton binding of standard SRHA.[46]

TiO₂ charge concentrations were estimated based on manufacturer data (primary TiO₂ diameter equal to 15 nm and in good agreement with the mode value of TiO₂ number size distribution (ESI† Fig. S1)) to calculate the S_A and on the study by Kominami *et al.* to estimate σ_{TiO_2}.[47] A value of S_A equal to 100 m² g⁻¹ and 5 sites per nm² σ_{TiO_2} were used to determine the TiO₂ charge concentration, and the factor of conversion between the mass and the charge concentration was set so that a 1 g L⁻¹ TiO₂ dispersion corresponds to a 0.83 mM charge concentration.

The mixing order of the two compounds, which is an important issue to consider, was investigated to better understand the TiO₂–SRHA and SRHA–TiO₂ interactions and agglomeration process as illustrated in Fig. 1. In the first set of experiments (type I) SRHA played the role of ligand and was added to the TiO₂ dispersions. In the second set of experiments (type II) TiO₂ ENPs (L) were added to SRHA (M).

Experiments were made at pH 3.8 (and at pH 10.4) without the addition of electrolyte. Such a pH value was used to address the interaction between isolated and SRHA. It is important to note that results remain valid as long as pH < pH_{PCN,TiO_2}. The domain of concentration investigated was from 0.25 mM SRHA in 0.1 g L⁻¹ TiO₂ to 1.25 mM SRHA in 0.5 g L⁻¹ TiO₂ for type I experiments and from 0.7 g L⁻¹ TiO₂ in 0.0375 mM SRHA to 3.5 g L⁻¹ TiO₂ in 0.1875 mM alginate for type II experiments. Such TiO₂ concentrations are higher than the expected environmental concentrations, which are in the ng L⁻¹ to μg L⁻¹ range,[8–10] but necessary to obtain an optimum signal with the calorimeter.

2.3. Zeta potential and size distribution measurements

Zeta (ζ) potential values and z-average hydrodynamic diameters of TiO₂ and SRHA suspensions as a function of pH as well as TiO₂ in the presence of SRHA as a function of charge ratio were determined by laser Doppler velocimetry and dynamic light scattering (Zetasizer Nano ZS instrument, Malvern Instruments, Worcestershire, UK). The instrument was operated at 298.15 K. For the determination of ζ potential values the Smoluchowski approximation model was applied according to the formation and presence of large agglomerates.[30] All polydispersity indexes were found to be below 0.6.

3. Results and discussion

ITC experiments were realized to determine the binding properties mainly at pH < pH_{PCN,TiO_2}. Such a pH domain favors electrostatic interactions. TiO₂ ENPs are positively charged (ζ potential = +40.9 ± 1.4 mV) (mean ± standard deviation on mean of triplicates), whereas SRHAs are negatively charged (ζ potential = −37.2 ± 1.9 mV) as shown in Fig. 2, where the ζ potential is represented as a function of pH for both compounds. Some experiments were also made at pH > pH_{PCN,TiO_2}, where both compounds exhibit the same charge (negatively charged TiO₂ and SRHA) to check if only steric and electrostatic repulsions are involved or if other forces such as van der Waals interactions are also expected to play a significant role during the interaction processes. At pH < pH_{PCN,TiO_2} and pH > pH_{PCN,TiO_2} TiO₂ ENPs are dispersed as shown in Fig. S1† with z-average diameter equal to 50 nm, whereas the SRHA z-average diameter is found to be constant with pH changes and equal to 379 ± 19 nm (Fig. S2†).

3.1. TiO₂–SRHA thermodynamic and reaction binding parameters determined by ITC

3.1.1. Type I titration – addition of SRHA in TiO₂ dispersions. At pH < pH_{PCN,TiO_2}, when SRHAs are added to TiO₂, the interactions are found to be important, as shown in the real-time thermogram in Fig. 3a where the titration process for a 0.1 g L⁻¹ TiO₂ dispersion with 0.25 mM SRHA is addressed. Negative peaks in the thermogram indicate that the interaction between TiO₂ and SRHA is an exothermic
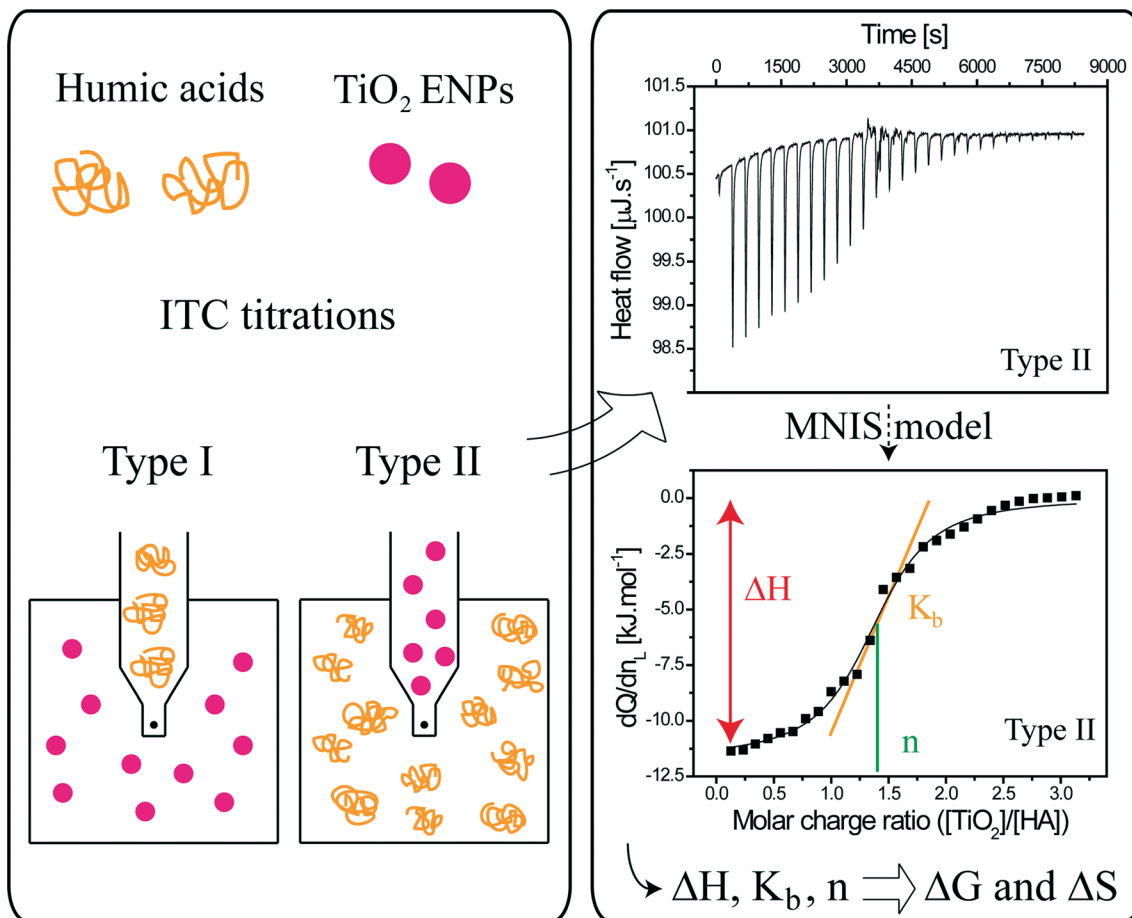
This journal is © The Royal Society of Chemistry 2015

Environ. Sci.: Nano, 2015, **2**, 541–550 | 543

Fig. 1 ITC type I (SRHA in TiO$_2$ dispersion) and type II (TiO$_2$ in SRHA) titrations. ITC measurements give the heat flow for each of the 28 injections, and after fitting the integrated data with the multiple non-interacting sites (MNIS) model the enthalpy of exchange ΔH, the binding constant K_b and the reaction stoichiometry n are determined. It allows the calculation of the entropy ΔS and total free energy ΔG for TiO$_2$–SRHA interaction.
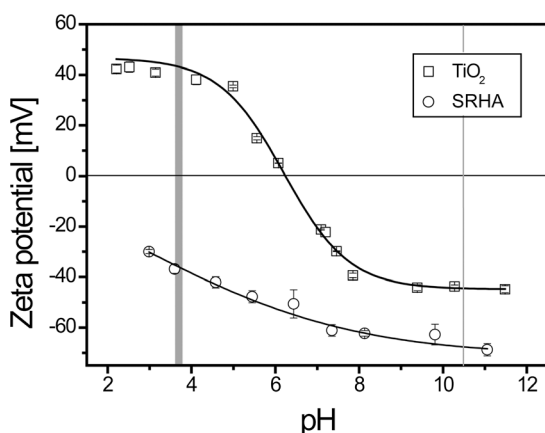

Fig. 2 Zeta potential values of TiO$_2$ (open squares) and SRHA (open circles) as a function of pH. TiO$_2$ isoelectric point is found here to be equal to 6.2 ± 0.1, whereas SRHAs exhibit a negative structural charge in the full pH range. At pH 3.1 TiO$_2$ and alginate have ζ potential values equal to +40.9 ± 1.4 mV and −37.2 ± 1.9 mV, respectively (large gray vertical line). At pH 10.4 both compounds are negatively charged (narrow gray vertical line). [TiO$_2$] = 50 mg L^{-1}, [SRHA] = 100 mg L^{-1} and [NaCl] = 0.001 M.

process since the thermogram represents the power generated by the calorimeter along the titration to maintain a small and constant difference in temperature between a reference cell (filled with the reaction solvent: water) and the reaction cell, both being located in an adiabatic jacket. After the first injection, corresponding to the peak of smaller intensity (as the injected volume here is equal to 2 μL of SRHA instead of the 10 μL "conventional" injection volumes), the next 15 peak intensities (each peak is referring to a single injection) are of similar value. This denotes that, in such condition, a large number of free sites are available on TiO$_2$ ENP surface for SRHA adsorption. Then, as the titration is progressing, the peak intensities are decreasing due to the restriction of the TiO$_2$ binding site available for further SRHA adsorption until site saturation is reached. Then mainly dilution effect is observed as shown by the low heat flow recorded by the calorimeter. Fig. 3b represents the energy of exchange per mole of injectant (dQ/dn_L) as a function of SRHA over TiO$_2$ charge ratio (Z = [L]/[M]) and is obtained by integration of the previous thermogram. The plot is then fitted with the MNIS model to determine the thermodynamic and reaction parameters associated to the interaction
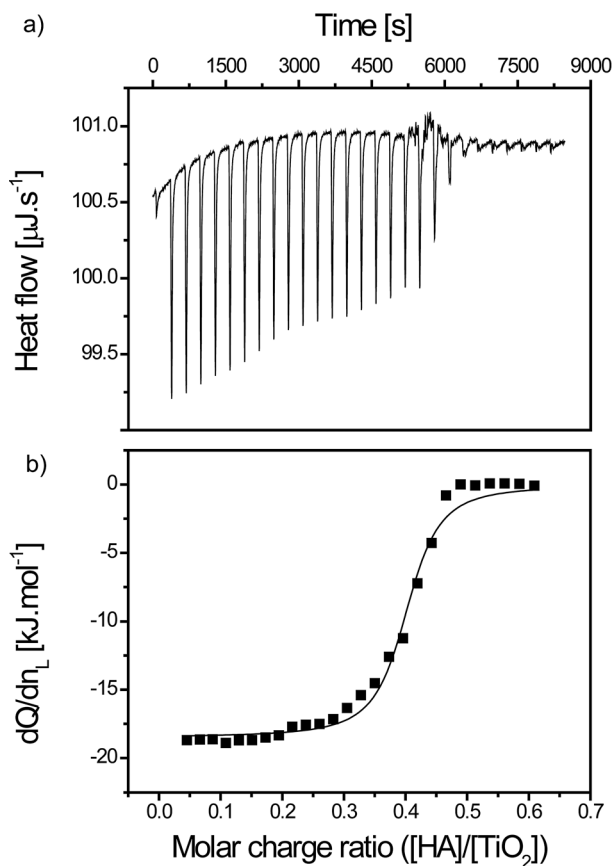
544 | *Environ. Sci.: Nano*, 2015, **2**, 541–550

This journal is © The Royal Society of Chemistry 2015

a)

b)

Fig. 3 a) Real-time thermogram for TiO₂ 0.1 g L⁻¹ titration with SRHA 0.25 mM at pH <pH$_{PCN,TiO_2}$ and at 298.15 K. The heat flow refers to the thermal compensation of the calorimeter to keep the sample at a constant temperature. Here negative peaks indicate an exothermic reaction. After about 20 injections site saturation occurs and only weak binding energy is observed. b) The respective integrated heat data (dQ/dn_L) as a function of molar charge ratio ([SRHA]/[TiO₂]) is fitted with the multiple non-interacting sites (MNIS) model. The binding enthalpy, the binding constant and the reaction stoichiometry are −18.3 kJ mol⁻¹, 4.3 × 10⁶ M⁻¹ and 0.41, respectively.

process.[44] The interaction process, for the titration of a 0.1 g L⁻¹ TiO₂ dispersion with a 0.25 mM SRHA solution, is exothermic, as ΔH_b is equal to −18.3 kJ mol⁻¹. The binding affinity between the ENPs and SRHA, which is expressed by K_b, is equal to 4.3 × 10⁶ M⁻¹. The reaction stoichiometry is found to be equal to 0.41. The fitting parameters allow the calculation of ΔG and ΔS which are equal to −37.9 kJ mol⁻¹ and 65.8 J K⁻¹ mol⁻¹, respectively. Three other type I experiments were done at different concentrations but by keeping the ratio between TiO₂ and SRHA concentrations constant in order to

evaluate the influence of relative concentration on the interaction processes. The real-time thermograms and the plots of the heat exchange as a function of SRHA over TiO₂ charge ratio for these experiments are presented in Fig. S3 to S5.† All determined and calculated thermodynamic and reaction parameters are presented in Table 1. To clearly see the main driving force (enthalpy versus entropy) the values of $T\Delta S$ are given in this table.

TiO₂ titrations with SRHA are thus spontaneous reactions with high Gibbs energy value ($\Delta G < -30$ kJ mol⁻¹). The interaction energies are found to lead to the formation of TiO₂–SRHA complexes due to favorable enthalpy conditions ($\Delta H_b < 0$) and entropic gain ($T\Delta S > 0$). Relative concentration is found to influence the binding energy as higher concentration involved higher ΔH_b values. This behavior can be attributed to the importance of SRHA homoagglomeration ("self"-assembly) due to agglomerates weakly bonded by hydrophobic interactions and H-bonding,[48,49] which is concentration dependent.[50] Indeed larger SRHA agglomerates are expected to promote interaction with an increasing amount of TiO₂ ENPs in comparison to smaller SRHA agglomerates. The decrease in the binding affinity, and thus calculated Gibbs free energy, with the increase in the relative experimental concentrations is due to the relation between K_b and c according to $K_b \sim c^{-2}$.[44] The reaction stoichiometry is found, for type I titrations, to slightly decrease. Overall it denotes that TiO₂ ENPs are not fully coated with SRHA, which is in agreement with the SRHA structure. Indeed humic acids are often considered as heterogeneous semi-rigid globular macromolecules.[51–53] The entropy gain is lower when relative concentrations are increasing. This is not only due to the decrease in the Gibbs free energy for higher concentration but also to the fact that for larger SRHA homoagglomerates the gain in entropy is smaller owing to the lower conformational entropy gain that occurs during the binding process and lower gain in entropy due to the release of water molecules. The complex formation is therefore mainly driven by the importance of the binding energy ($\Delta H_b < -T\Delta S$) except for the lowest relative concentration investigated in this study for which ΔH_b and $-T\Delta S$ have similar values.

3.1.2. Type II titration – addition of TiO₂ in SRHA solutions. Fig. 4 represents the real-time thermogram and the respective integrated heat of exchange per mol of TiO₂ as a function of molar charge ratio for 0.7 g L⁻¹ TiO₂ in 0.0375 mM SRHA. When SRHA is titrated with TiO₂ ENPs at pH <pH$_{PCN,TiO_2}$, the interaction process is also entropically and enthalpically favorable. Indeed ΔH_b and $T\Delta S$ are equal to

Table 1 Fitting parameters ΔH_b, K_b and n from ITC analysis of the integrated heats with the MNIS model and calculated ΔG and $T\Delta S$ (from K_b and ΔH_b values) for type I titration

SRHA in TiO₂	ΔH_b [kJ mol⁻¹]	K_b [M⁻¹]	n	ΔG [kJ mol⁻¹]	$T\Delta S$ [kJ mol⁻¹]
0.25 mM in 0.1 g L⁻¹	−18.3	4.3 × 10⁶	0.41	−37.9	19.6
0.50 mM in 0.2 g L⁻¹	−22.9	2.5 × 10⁶	0.31	−36.5	13.6
0.75 mM in 0.3 g L⁻¹	−23.2	1.1 × 10⁶	0.34	−34.6	11.4
1.25 mM in 0.5 g L⁻¹	−24.4	8.5 × 10⁵	0.32	−33.9	9.4

This journal is © The Royal Society of Chemistry 2015
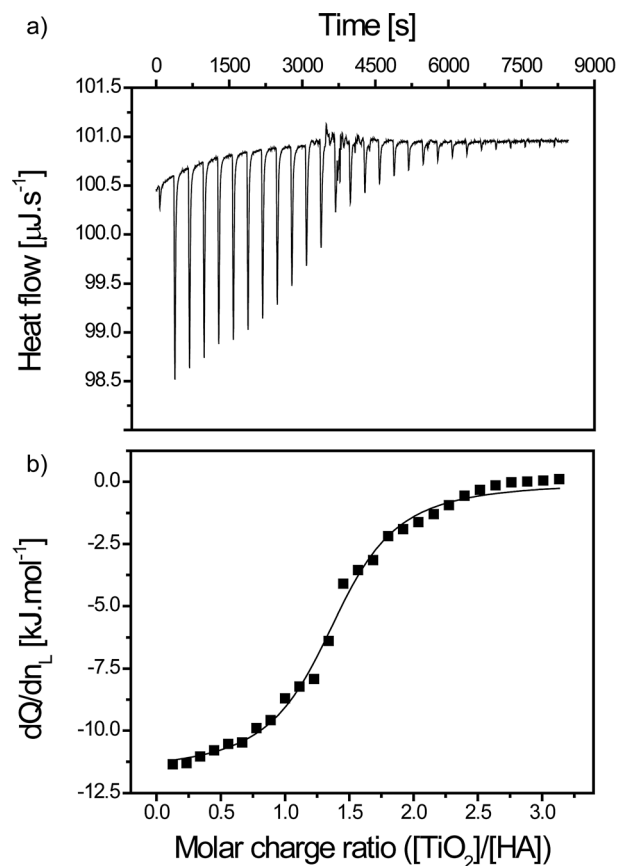
Environ. Sci.: Nano, 2015, **2**, 541–550 | **545**

Fig. 4 a) Real-time thermogram for SRHA 0.0375 mM titration with TiO$_2$ 0.7 g L^{-1} at pH <pH$_{PCN,TiO_2}$ and at 298.15 K. Negative peaks indicate an exothermic reaction and after about 20 injections site saturation occurs and only weak binding energy is observed. b) The respective integrated heat data as a function of TiO$_2$ over SRHA molar charge ratio is fitted with the MNIS model. The binding enthalpy, the binding constant and the reaction stoichiometry are −11.7 kJ mol^{-1}, 5.1 × 10^5 M^{-1} and 1.41, respectively.

−11.7 kJ mol^{-1} and 20.9 kJ mol^{-1}, respectively. A binding constant of 5.1 × 10^5 in the more diluted conditions and a 1.41 reaction stoichiometry suggest an important binding affinity and non fully coated TiO$_2$ ENPs. Experiments at different concentrations are also realized and all parameters are presented in Table 2. Real-time thermograms and respective heat exchange plots are presented in Fig. S6 to S8.†

The reaction stoichiometry is not dependent on the relative concentration investigated (n = 1.41 ± 0.15). Moreover, the enthalpy of binding is not significantly influenced by the increase in concentration (−12.3 ± 0.8 kJ mol^{-1}).

When comparison is made between the two titration procedures an important difference in the value of the binding enthalpy is observed due to the much higher SRHA concentration, and thus larger SRHA homoagglomerate formation and higher enthalpy of interaction for type I. When SRHAs are added to the solution containing TiO$_2$ the enthalpy is significantly more important because of the possibility to complex more ENPs. SRHA homoagglomeration phenomenon is also the reason why type I titrations are mainly driven by enthalpy, whereas type II interaction processes are driven by an important gain in entropy as the total free Gibbs free energy is similar for both titration types. The entropic gain arises from the SRHA and ENP counter-ions and water molecules released during the adsorption processes. It should be noted that larger loss of entropy is associated with a larger increase in enthalpy as suggested by the enthalpy–entropy compensation.[54,55] Similar total free energy values were observed during the association process between ZnO ENPs with lysozyme as well as between proteins and amino acid functionalized gold ENPs.[56–58] However, in these studies the interactions (K_b = 0.9 × 10^6 M^{-1}) were enthalpically favorable but entropically unfavorable due to conformational restriction of proteins.

Reaction stoichiometries are not equal to unity even in the presence of an electrostatic interaction scenario. Indeed as SRHAs are relatively heterogeneous in size and highly charged macromolecules in these working conditions, bridging and patch mechanisms are expected to play an important role during the interaction processes.[59–61] Therefore a significant number of ENP surface sites are hindered due to conformational restrictions and surface charge heterogeneity, which favors a reaction stoichiometry lower than unity for type I titration and higher than unity for type II.

Another interesting behavior when investigating the association process between TiO$_2$ and SRHA is the weak exchange energy which is still observed for high [L] over [M] charge ratio. It means that non-electrostatic interactions are involved even if EPN surface sites are no longer available. Such interaction energies, which are more important for high SRHA concentrations, can be linked to the amphiphilic character of SRHA that is known to exhibit significant van der Waals interactions.[62]

To verify the presence of such van der Waals interactions, the complexation process between TiO$_2$ and SRHA is also investigated at pH 10.4 for the titration of a 5 g L^{-1} TiO$_2$ dispersion with 1.25 mM SRHA. At pH >pH$_{PCN,TiO_2}$ both compounds are negatively charged (Fig. 2). If only electrostatic

Table 2 Fitting parameters ΔH_b, K_b and n from ITC analysis of the integrated heats with the MNIS model and calculated ΔG and $T\Delta S$ (from K_b and ΔH_b values) for type II titration

TiO$_2$ in SRHA	ΔH_b [kJ mol^{-1}]	K_b [M^{-1}]	n	ΔG [kJ mol^{-1}]	$T\Delta S$ [kJ mol^{-1}]
0.7 g L^{-1} in 0.0375 mM	−11.7	5.1 × 10^5	1.41	−32.6	20.9
1.4 g L^{-1} in 0.0750 mM	−12.0	3.3 × 10^5	1.60	−31.5	19.5
2.1 g L^{-1} in 0.1125 mM	−12.2	2.5 × 10^5	1.40	−30.8	18.6
3.5 g L^{-1} in 0.1875 mM	−13.4	1.6 × 10^5	1.24	−29.6	16.2

546 | *Environ. Sci.: Nano*, 2015, **2**, 541–550

This journal is © The Royal Society of Chemistry 2015

interactions are involved during the association processes the real-time thermograms and the respective heat exchange plots for both the titration (1.25 mM SRHA in 5 g L^{-1}) and for the dilution (1.25 mM SRHA in water) should be identical (or at least very similar). This is not the case and an association process is shown to happen between TiO_2 and SRHA in this unfavorable electrostatic scenario (Fig. S9 and S10†). van der Waals interactions are shown to be significant with energy exchange in the early titration stage, three times greater than the dilution effect and of the order of a few kJ mol^{-1}. The presence of van der Waals interactions at pH >pH$_{PCN,TiO_2}$ is also in good agreement with a previous study where SRHAs were shown to be adsorbed onto TiO_2 ENPs with a decrease in the electrophoretic mobility and an increase in ENP size when negatively charged SRHAs were added to negatively charged TiO_2.[63]

3.2. Effect of TiO_2–SRHA agglomeration and surface charge on binding heat of exchange

In order to understand the influence of agglomerate formation and surface charge on the heat of exchange between TiO_2 and SRHA, electrophoretic mobility measurements and size determination were realized and then comparison was made with the previous heat exchange data plots obtained by ITC. Experiments were realized at pH <pH$_{PCN,TiO_2}$ for 0.25 mM SRHA in 0.1 g L^{-1} TiO_2 (type I) and 0.7 g L^{-1} TiO_2 in 0.0375 mM SRHA (type II) with a 300 s delay between each successive titrant addition (identical to that for ITC experiments). As this delay time was not long enough to perform both ζ potential and z-average diameter determination, triplicates for each of these parameters were measured separately.

Type I titration. ζ potential value and binding heat of exchange as a function of SRHA over TiO_2 charge ratio are represented in Fig. 5a. For the first 15th SRHA addition (Z = [L]/[M] <0.35) the binding enthalpy slightly decreases in this domain concomitantly with ζ potential, which exhibits the same behavior due to the adsorption of negatively charged SRHAs onto positively charged TiO_2 ENPs. It means that a large number of TiO_2 surface sites are still available for SRHA adsorption. Then a drastic decrease in the exchange energy is observed due to important surface charge modification leading to ENP charge inversion (−4.7 ± 0.4 mV) for Z = 0.4. After charge inversion has occurred, the energy of interaction is much lower due to electrostatic repulsions between the TiO_2–SRHA complexes and the titrant (SRHA) until the change in enthalpy is found to be constant for ζ potential values greater than −10 mV. Size evolution as a function of molar charge ratio (Fig. 5b) is in good agreement with our observations. For Z <0.4 the adsorption of SRHA on TiO_2 leads to the formation of agglomerates due to patch and bridging mechanisms with a linear increase in the z-average diameter value. Once charge neutralization and then charge inversion are achieved the formation of large agglomerates (554 ± 28 nm) is observed. This sudden change in the agglomerate size corresponds to an important physical change (precipitation)
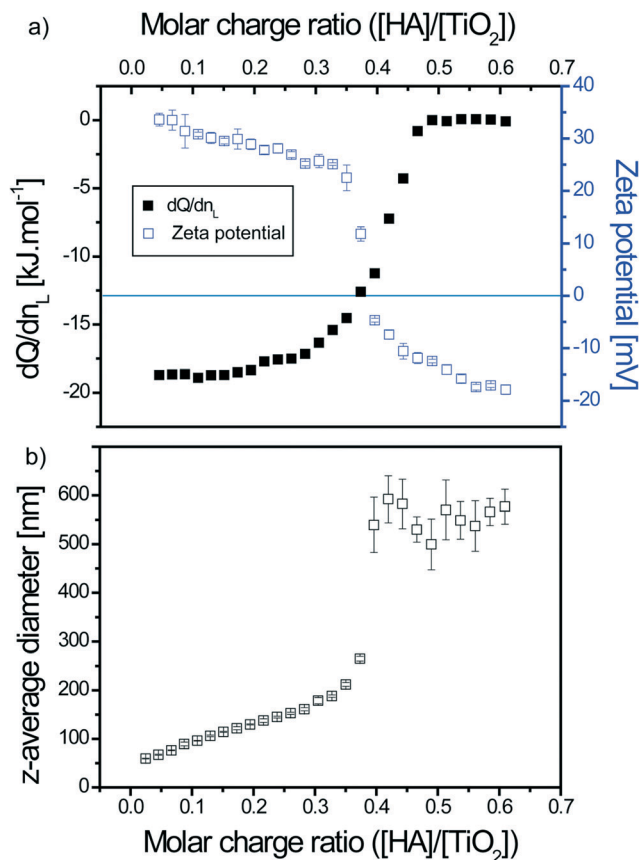

Fig. 5 a) Integrated heat data and ζ potential values as a function of SRHA over TiO_2 charge ratio for TiO_2 0.1 g L^{-1} titration with SRHA 0.25 mM at pH < pH$_{PCN,TiO_2}$. For a ratio up to 0.35, the binding enthalpy and the ζ potential values are slightly decreasing. Then charge inversion (ζ potential = −4.7 ± 0.4 mV) is observed for Z = 0.40 and for Z > 0.48 site saturation occurs and weak and constant interaction are observed. b) z-average diameter as a function of molar charge. Strong TiO_2 ENPs destabilization occurs for Z > 0.35 whereas, below this ratio, the increase in z-average diameter is linear, indicating ENPs bridging.

after charge inversion has occurred. This change is also detected in the real-time thermogram (Fig. 3) by a specific signature where important fluctuations of the heat flow are recorded (observed at the baseline level).

Type II titration. ζ potential value and binding energy as a function of TiO_2 over SRHA charge ratio are presented in Fig. 6a. The influence of the charge modification on the heat exchange is clearly observed since the enthalpy of binding decrease is dependent on the surface charge and follows the decrease in ζ potential. For a charge ratio less than 1.25, ζ potential values are higher than −20 mV and the respective heat of exchange is larger than −8 kJ mol^{-1}. Then further addition of TiO_2 induced the charge inversion of the TiO_2–SRHA complexes and thus an important decrease in the energy of association, which becomes constant for ζ potential values higher than +25 mV. z-average diameter value as a function of molar charge ratio is shown in Fig. 6b. Before charge inversion the sizes of the complexes are slowly
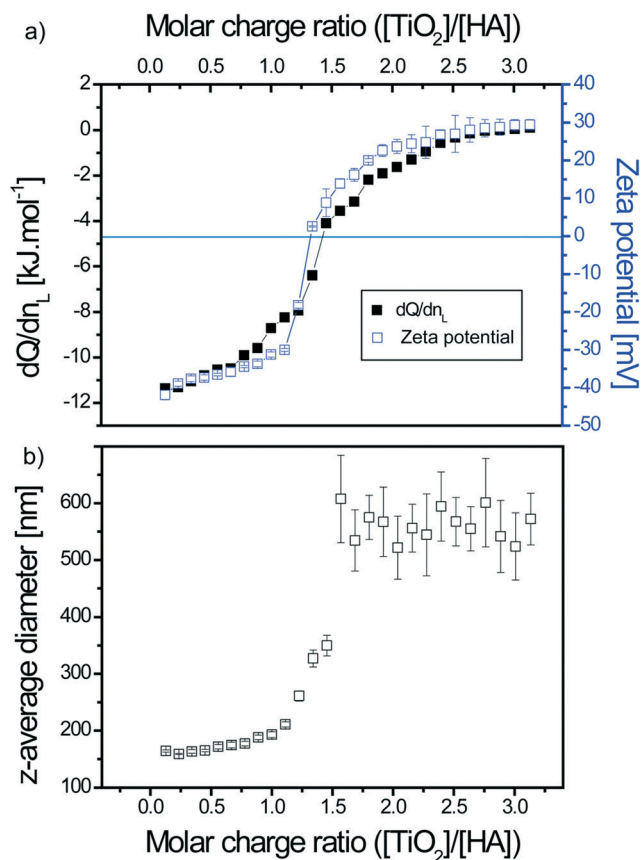
This journal is © The Royal Society of Chemistry 2015

Environ. Sci.: Nano, 2015, 2, 541–550 | 547

a)

Fig. 6 a) Integrated heat data and ζ potential values as a function of TiO$_2$ over SRHA charge ratio for an SRHA 0.0375 mM titration with TiO$_2$ 0.7 g L^{-1} at pH $<$pH$_{PCN,TiO_2}$. For a charge ratio $\geq$1.25, charge inversion is observed (ζ potential = +2.6 ± 0.2 mV) and only weak interactions are observed. b) z-average diameter as a function of molar charge. Strong TiO$_2$ ENPs destabilization occurs for Z >1.5, whereas below this ratio, z-average diameter increase is linear, indicating ENP bridging.

increasing due to patch and bridging mechanisms. Then charge neutralization and further inversion lead to the formation of large agglomerates (562 ± 27 nm for Z >1.5).

For both titration types, good agreement is found between the surface charge modification of TiO$_2$–SRHA complexes, the heat of exchange associated to the interaction processes and the size evolution along the titrations. An interesting behavior for the interaction of TiO$_2$ ENPs in the presence of SRHA is that non-negligible binding enthalpy is observed even after charge inversion (and particle precipitation) has occurred. It denotes the role of van der Waals interactions (especially for type I) and change of conformation of SRHA. Such a behavior is not observed when linear natural polysaccharides (alginate) are considered.[64] This is due to the alginate chemical properties for which van der Waals interactions are not favored. Dynamic light scattering has also permitted assignment of the real-time thermogram signature to an important precipitation domain in agreement with z-average diameter and ζ potential values.

4. Conclusion

The spontaneous association process between TiO$_2$ nanoparticles and Suwannee River humic acids has been shown to be dependent on concentration and mixing order. All interaction processes were found favorable from an enthalpic and entropic point of view and agglomeration was shown to be promoted by patch and bridging mechanisms.

This study shows the high potential of isothermal titration calorimetry (ITC) for the investigation of interactions between engineered nanoparticles (ENPs) and natural organic matter. Indeed ITC, especially when associated with light scattering techniques, not only allows the determination of important thermodynamic (ΔH, ΔG and ΔS) and reaction (K_b and n) parameters but also a better understanding of the mechanism of interactions (and/or agglomeration) and the forces (hydrophobic, electrostatic) involved during association processes. ITC also gives quantitative and accurate information on the adsorption energies and hence potential reversibility of nanoparticle coating processes in various conditions. This novel technique in environmental nanoscience also constitutes a potential promising instrumental method for the investigation of competitive sorption of environmental compounds (natural organic molecules and inorganic colloids) on ENPs. The major limitations of ITC concern not only the time-consuming sample preparation and long analysis time but also the high concentrations needed (especially for the titrant) which can be a problem if working with costly materials or molecules being concentration conformational dependent. Nevertheless, ITC is a non-destructive technique which allow the quantification of the interfacial reactions (and the possible reversibility and stability of the association processes), which is essential fundamental information for a better holistic understanding of the transport and fate of (nano)particles in aquatic systems when exposed to a broad range of molecules of different abundance.

Acknowledgements

References

1 S. J. Klaine, P. J. J. Alvarez, G. E. Batley, T. F. Fernandes, R. D. Handy, D. Y. Lyon, S. Mahendra, M. J. McLaughlin and J. R. Lead, *Environ. Toxicol. Chem.*, 2008, **27**, 1825–1851.

548 | *Environ. Sci.: Nano*, 2015, **2**, 541–550

This journal is © The Royal Society of Chemistry 2015

2   Y. Ju-Nam and J. R. Lead, *Sci. Total Environ.*, 2008, **400**, 396–414.

3   P. Biswas and C. Y. Wu, *J. Air Waste Manage. Assoc.*, 2005, **55**, 708–746.

4   M. R. Wiesner, G. V. Lowry, P. Alvarez, D. Dionysiou and P. Biswas, *Environ. Sci. Technol.*, 2006, **40**, 4336–4345.

5   G. V. Lowry, K. B. Gregory, S. C. Apte and J. R. Lead, *Environ. Sci. Technol.*, 2012, **46**, 6893–6899.

6   F. Piccinno, F. Gottschalk, S. Seeger and B. Nowack, *J. Nanopart. Res.*, 2012, **14**, 1109.

7   M. Auffan, J. Rose, J.-Y. Bottero, G. V. Lowry, J.-P. Jolivet and M. R. Wiesner, *Nat. Nanotechnol.*, 2009, **4**, 634–641.

8   G. E. Batley, J. K. Kirby and M. J. McLaughlin, *Acc. Chem. Res.*, 2013, **46**, 854–862.

9   N. Sani-Kast, M. Scheringer, D. Slomberg, J. Labille, A. Praetorius, P. Ollivier and K. Hungerbühler, *Sci. Total Environ.*, 2015, **535**, 150–159.

10 F. Gottschalk, T. Sonderer, R. W. Scholz and B. Nowack, *Environ. Sci. Technol.*, 2009, **43**, 9216–9222.

11 R. A. French, A. R. Jacobson, B. Kim, S. L. Isley, R. L. Penn and P. C. Baveye, *Environ. Sci. Technol.*, 2009, **43**, 1354–1359.

12 J. Labille and J. Brant, *Nanomedicine*, 2010, **5**, 985–998.

13 B. Mukherjee and J. W. Weaver, *Environ. Sci. Technol.*, 2010, **44**, 3332–3338.

14 I. Chowdhury, S. L. Walker and S. E. Mylon, *Environ. Sci.: Processes Impacts*, 2013, **15**, 275–282.

15 M. J. Mulvihill, S. E. Habas, I. Jen-La Plante, J. Wan and T. Mokari, *Chem. Mater.*, 2010, **22**, 5251–5257.

16 C. Levard, E. M. Hotze, G. V. Lowry and G. E. Brown Jr., *Environ. Sci. Technol.*, 2012, **46**, 6900–6914.

17 A. A. Keller, H. Wang, D. Zhou, H. S. Lenihan, G. Cherr, B. J. Cardinale, R. Miller and Z. Ji, *Environ. Sci. Technol.*, 2010, **44**, 1962–1967.

18 B. Collin, M. Auffan, A. C. Johnson, I. Kaur, A. A. Keller, A. Lazareva, J. R. Lead, X. Ma, R. C. Merrifield, C. Svendsen, J. C. White and J. M. Unrine, *Environ. Sci.: Nano*, 2014, **1**, 533–548.

19 N. von Moos, P. Bowen and V. I. Slaveykova, *Environ. Sci.: Nano*, 2014, **1**, 214–232.

20 E. M. Thurman and R. L. Malcolm, *Environ. Sci. Technol.*, 1981, **15**, 463–466.

21 M. N. Jones and N. D. Bryan, *Adv. Colloid Interface Sci.*, 1998, **78**, 1–48.

22 M. Belen Romanello and M. M. Fidalgo de Cortalezzi, *Water Res.*, 2013, **47**, 3887–3898.

23 M. Erhayem and M. Sohn, *Sci. Total Environ.*, 2014, **468–469**, 249–257.

24 J. A. Gallego-Urrea, J. Perez Holmberg and M. Hassellov, *Environ. Sci.: Nano*, 2014, **1**, 181–189.

25 S. M. Louie, R. D. Tilton and G. V. Lowry, *Environ. Sci. Technol.*, 2013, **47**, 4245–4254.

26 X. Liu, M. Wazne, Y. Han, C. Christodoulatos and K. L. Jasinkiewicz, *J. Colloid Interface Sci.*, 2010, **348**, 101–107.

27 M.-H. Shen, Y.-G. Yin, A. Booth and J.-F. Liu, *Water Res.*, 2015, **71**, 11–20.

28 F. Mohd Omar, H. Abdul Aziz and S. Stoll, *Sci. Total Environ.*, 2014, **468–469**, 195–201.

29 F. Loosli, P. Le Coustumer and S. Stoll, *Environ. Sci.: Nano*, 2014, **1**, 154–160.

30 M. Baalousha, *Sci. Total Environ.*, 2009, **407**, 2093–2101.

31 L. Vitorazi, N. Ould-Moussa, S. Sekar, J. Fresnais, W. Loh, J. P. Chapel and J. F. Berret, *Soft Matter*, 2014, **10**, 9496–9505.

32 I. Jelesarov and H. R. Bosshard, *J. Mol. Recognit.*, 1999, **12**, 3–18.

33 W. Kim, Y. Yamasaki, W.-D. Jang and K. Kataoka, *Biomacromolecules*, 2010, **11**, 1180–1186.

34 J. E. Ladbury, *Thermochim. Acta*, 2001, **380**, 209–215.

35 C. O. Hendren, X. Mesnard, J. Droege and M. R. Wiesner, *Environ. Sci. Technol.*, 2011, **45**, 2562–2569.

36 K. Schmid and M. Riediker, *Environ. Sci. Technol.*, 2008, **42**, 2253–2260.

37 J. Labille, J. Feng, C. Botta, D. Borschneck, M. Sammut, M. Cabie, M. Auffan, J. Rose and J.-Y. Bottero, *Environ. Pollut.*, 2010, **158**, 3482–3489.

38 X. Chen and S. S. Mao, *Chem. Rev.*, 2007, **107**, 2891–2959.

39 A. Weir, P. Westerhoff, L. Fabricius, K. Hristovski and N. von Goetz, *Environ. Sci. Technol.*, 2012, **46**, 2242–2250.

40 F. Gottschalk, T. Sun and B. Nowack, *Environ. Pollut.*, 2013, **181**, 287–300.

41 X. Liu, G. Chen, A. A. Keller and C. Su, *Environ. Sci.: Processes Impacts*, 2013, **15**, 169–189.

42 B. J. R. Thio, D. Zhou and A. A. Keller, *J. Hazard. Mater.*, 2011, **189**, 556–563.

43 C. Guéguen and C. W. Cuss, *J. Chromatogr. A*, 2011, **1218**, 4188–4198.

44 J. Courtois and J. F. Berret, *Langmuir*, 2010, **26**, 11750–11758.

45 http://www.humicsubstances.org/elements.html - Accessed May 3, 2015.

46 J. D. Ritchie and E. M. Perdue, *Geochim. Cosmochim. Acta*, 2003, **67**, 85–96.

47 H. Kominami, M. Itonaga, A. Shinonaga, K. Kagawa, S. Konishi and Y. Kera, in *Preparation of vanadium-based catalysts for selective catalytic reduction of nitrogen oxides using titania supports chemically modified with organosilanes*, ed. S.i. S. S. a. Catalysis, Elsevier, 2000, vol. 143, pp. 1089–1096.

48 J. A. Leenheer and J. P. Croue, *Environ. Sci. Technol.*, 2003, **37**, 18A–26A.

49 P. Conte and A. Piccolo, *Environ. Sci. Technol.*, 1999, **33**, 1682–1690.

50 D. Smejkalova and A. Piccolo, *Environ. Sci. Technol.*, 2008, **42**, 699–706.

51 J. Buffle, *Complexation reactions in aquatic systems: an analytical approach*, Ellis Horwood, Chichester, 1988.

52 J. Buffle, K. J. Wilkinson, S. Stoll, M. Filella and J. W. Zhang, *Environ. Sci. Technol.*, 1998, **32**, 2887–2899.

53 H.-R. Schulten, P. Leinweber and M. Schnitzer, *Structure and Surface Reactions of Soil Particles*, ed. M. Huang, N. Senesi and J. Buffle, Wiley, New York, 1998, pp. 281–324.

54 V. Ravi, J. M. Binz and R. M. Rioux, *Nano Lett.*, 2013, **13**, 4442–4448.

This journal is © The Royal Society of Chemistry 2015

Environ. Sci.: Nano, 2015, **2**, 541–550 | 549

55 M. S. Searle and D. H. Williams, *J. Am. Chem. Soc.*, 1992, **114**, 10690–10697.

56 T. Chatterjee, S. Chakraborti, P. Joshi, S. P. Singh, V. Gupta and P. Chakrabarti, *FEBS J.*, 2010, **277**, 4184–4194.

57 S. Chakraborti, T. Chatterjee, P. Joshi, A. Poddar, B. Bhattacharyya, S. P. Singh, V. Gupta and P. Chakrabarti, *Langmuir*, 2010, **26**, 3506–3513.

58 M. De, C.-C. You, S. Srivastava and V. M. Rotello, *J. Am. Chem. Soc.*, 2007, **129**, 10747–10753.

59 J. Gregory, Flocculation by polymers and polyelectrolytes, *Solid/liquid dispersions*, Academic Press, London, 1987.

60 M. Elimelech, J. Gregory, X. Jia and R. A. Williams, *Particle deposition and aggregation: Measurement, modeling, and simulation*, Butterworth-Heinemann Ltd, Oxford, 1995.

61 J. Gregory, *J. Colloid Interface Sci.*, 1973, **42**, 448–456.

62 E. Tombacz, *Soil Sci.*, 1999, **164**, 814–824.

63 F. Loosli, P. Le Coustumer and S. Stoll, *Water Res.*, 2013, **47**, 6052–6063.

64 F. Loosli, L. Vitorazi, J.-F. Berret and S. Stoll, *Water Res.*, 2015, **80**, 139–148.